Development and application of a high resolution hybrid modelling system for the evaluation of urban air quality

N. Pepe[1,2], G. Pirovano[1], G. Lonati[2], A. Balzarini[1], A. Toppetti[1], G.M. Riva[1], M. Bedogni[3]

1 RSE Spa, via Rubattino 54 - 20134 Milano, Italy
2 Department of Civil and Environmental Engineering, Politecnico Milano, Milano, 20133, Italy
3 AMAT, via T. Pini 1, 20134 Milano, Italy

Corresponding author: Nicola Pepe, Tel: +390239925639, Fax: +3902239924608, E-mail: nicola.pepe@polimi.it, Via Rubattino 54 – 20134, Milano, Italy (Present address)

ABSTRACT

A hybrid modeling system (HMS) was developed to provide hourly concentrations at the urban local scale. The system is based on the combination of a meteorological model (WRF), a chemical and transport eulerian model (CAMx), which computes concentration levels over the regional domains, and a lagrangian dispersion model (AUSTAL2000), accounting for dispersion phenomena within the urban area due to local emission sources; a source apportionment algorithm is also included in the HMS in order to avoid the double counting of local emissions.

The HMS was applied over a set of nested domains, the innermost covering a 1.6x1.6 km^2 area in Milan city center with 20 m grid resolution, for NO_X simulation in 2010. For this paper the innermost domain was defined as "local", excluding usual definition of urban areas. WRF model captured the overall evolution of the main meteorological features, except for some very stagnant situations, thus influencing the subsequent performance of regional scale model CAMx. Indeed, CAMx was able to reproduce the spatial and temporal evolution of NO_X concentration over the regional domain, except a few episodes, when observed concentrations were higher than 100 ppb. The local scale model AUSTAL2000 provided high-resolution concentration fields that sensibly mirrored the road and traffic pattern in the urban domain. Therefore, the first important outcome of the work is that the application of the hybrid modelling system allowed a thorough and consistent description of urban air quality. This result represents a relevant starting point for future evaluation of pollution exposure within an urban context.

However, the overall performance of the HMS did not provide remarkable improvements with respect to stand-alone CAMx at the two only monitoring sites in Milan city center. HMS results were characterized by a smaller average bias, that improved about 6-8 ppb corresponding to 12-13% of the observed concentration, but by a lower correlation, that worsened around 1-3% (e.g. from 0.84 to 0.81 at Senato site), due to the concentration peaks produced by AUSTAL2000 during nighttime stable conditions. Additionally, the HMS results showed that it was unable to correctly take into account some local scale features (e.g. urban canyon effects), pointing out that the emission spatialization and time modulation criteria, especially those from road traffic, need further improvement.

Nevertheless, a second important outcome of the work is that some of the most relevant discrepancies between modeled and observed concentrations were not related to the horizontal resolution of the dispersion models but to larger scale meteorological features not captured by the meteorological model, especially during winter period. Finally, the estimated contribution of the local emission sources accounted on the annual average for about 25-30% of the computed concentration levels in the innermost urban domain. This confirmed that the whole Milan urban area as well as the outside background areas, accounting all sources outside the innermost domain, play a key role on air quality. The result suggests that strictly local emission policies could have a limited and indecisive effect on urban air quality, although this finding could be partially biased by model underestimation of the observed concentration.

Research Highlights

- Hybrid modeling system developed at the urban local scale
- Hourly model output at 20x20 m space resolution for urban area
- Improvement in model bias despite slightly worsened time correlation
- Weaknesses and strengths of the system are pointed out and discussed
- Estimated NO_X background accounted for about 75% in Milan area domain

Keywords: urban air quality; NO_x; hybrid modelling; CAMx; AUSTAL2000; Milan;

1. Introduction

The impact assessment of environmental policies on air quality involves reactive pollutants, thus requiring chemical transport models (CTMs) and urban to regional domains, depending by the area of interest (Isakov et al., 2007; Denby et al., 2011; Martins, 2012). Urban areas are composed by heterogeneous elements and present densely built-up features, which can influence the spatial distribution of some pollutants such as NOx and NO_2, as well as the primary fraction of PM (EEA, 2015; Torras Ortiz et al., 2013). Due to their relatively low spatial resolution, CTMs cannot capture correctly the strong spatial gradients that can take place in urban areas, hampering a reliable evaluation of human exposure (Isakov et al., 2009; Batterman et al., 2014). The reconstruction of air quality variability within urban areas would require local scale models (LSMs); nevertheless LSMs alone are usually unable to reproduce chemical reactions and can not be applied over large domains (Stein et al., 2007; Lefebvre et al., 2011; Beevers et al., 2012; Lefebvre et al., 2013; Isakov et al., 2014).
For all these reasons we developed an integrated hybrid modelling system (HMS) by combining the Comprehensive Air Quality Model (CAMx) with Extensions (Environ, 2011), as chemical transport model, and the AUSTAL2000 (Janicke consulting, 2014), as local scale model, according to a model nesting approach. The resulting HMS is a comprehensive and efficient modelling tool for urban air quality, capable of reconstructing the regional scale features of air pollution as well as the spatial variability of concentrations within urban areas, taking into account the building structures and the detailed spatial distribution of the emissions at the urban scale. In particular, this work is intended to define a standardized modelling chain that can use the same emission inventories and land use datasets, as well as meteorological inputs, for the CTM and LSM components of the HMS.
A case-study application of the HMS concerning the metropolitan area of Milan, with a specific focus over the city center, where the LSM was applied in cascade to the CTM in order to provide hourly NO_X concentration for a high resolution urban grid (20x20 m) for 2010, is presented and discussed.
The paper firstly describes the conceptual structure and the elements of the HMS. The following section is devoted to the evaluation of the performance of the CTM part of the HMS. Then the results of the LSM application are presented and compared with the corresponding CTM outcomes. HMS results at the Milan urban domain are then compared with observations. Finally the evaluation of the spatial variability of the fine scale concentrations is presented and discussed.

2. Methods

2.1. The hybrid modelling system

The hybrid system relies on two main components: the regional scale model CAMx and the local scale dispersion model AUSTAL2000. The modelling system also includes the Weather Research

and Forecasting (WRF) meteorological model and the SMOKE emission model. Interactions between all models are shown in the flow chart of Figure 1. All models and tools implemented in the modelling chain are based on open source codes. The modelling system has two main features:

- CTM and LSM input data consistency, i.e.: the two models share the same meteorological and emission data;
- solution to the double counting problem of local contribution, thanks to a source apportionment algorithm implemented in the CTM model the local sources' contribution is accounted for only by the LSM.

The modelling chain presents efficient features concerning computational time: 15 minutes/day with 8 core processors about CAMx outcomes while 4min/day about AUSTAL2000 outputs with single core. Physical and chemical processes are described and quantified although AUSTAL2000 treats all pollutants as inert. Chemical schemes are implemented into CAMx, as described in setting section, and cover an important role overall at the basin scale; conversely, at the local scale the correct quantification of the dispersion phenomena is more important in order to compute backlog events, key features concerning exposition levels within urban areas. Thanks to its LSM component the HMS can accurately reproduce the spatial pattern of emission sources and reconstruct the spatial variability of pollutants concentrations. Thus, for example, the HMS is helpful to define critical zones for urban pollution and to assess the impact of air quality control policies, as the introduction of "Low Emission Zone" (Hellison et al., 2013; Morfeld et al., 2014), popular in big cities of Germany and England and adopted also in Milan since a few years.

Models setup and details on the output of the HMS are given in the following paragraphs with specific reference to the case-study for NO_X concentration in Milan city center.

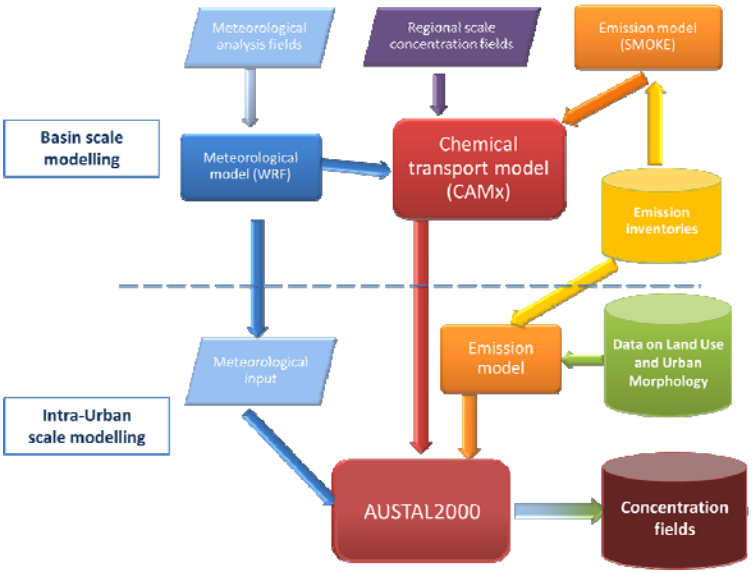

Figure 1. Flow chart of the hybrid modelling system

2.2. WRF setup

The WRF model v3.4.1 (Skamarock et al.,2008) was setup using 30 vertical layers, with the first one reaching about 25 meters from ground level; the top layer overcomes 15 km. Four horizontal nested grids were used, downscaling from a 3870x4140 km^2 domain covering Europe to a 1350x1530 km^2 domain over Italy, a 600x420 km^2 over the Po Valley and a 85x85 km^2 over a part of the Lombardy region, including the city of Milan. Each domain was gridded using different

resolutions starting from 45 km as grid step down to 15 km, 5 km and 1.7 km for the last domain. Initial and boundary conditions were taken from ECMWF analysis fields at 0.5x0.5° grid size, both at ground level and at different pressure levels (http://old.ecmwf.int/products/data/archive/ECMWF_catalogue/index.html). Data included 3D and surface parameters (wind speed components, temperature, relative humidity), 2D surface parameters (sea level pressure and temperature, separating sea cells from ground ones), 2D static parameter of land sea mask and 3D soil parameters (temperature and water content) integrated on 4 ground layers (0-7 cm, 7-28 cm, 28 cm-1m, 1-2.55 m). Main physical settings within WRF included the Rapid Radiation Transfer Model (RRTM) radiation scheme (Iacono et al., 2008), Morrison double moment microphysics processes scheme (Morrison et al., 2009), Yonsei University PBL scheme (Hong et al., 2006), Grell 3D scheme for clouding creation (Grell et al., 2002) over European and Italian domain, Monin-Obukhov surface layer scheme (Monin and Obukhov, 1954) and Noah land surface model (Chen and Dudhia, 2001). Analysis nudging of wind speed horizontal components, temperature and relative humidity was used in the WRF model with a nudging strength of $3x10^{-4}$. The classification system for land use was based on European database CORINE that counts 44 different categories (http://www.eea.europa.eu/), reclassified over 33 classes of USGS system. Particularly, CORINE adopts five different sub-categories of urban land use, from continuous urban fabric to discontinuous low-density urban fabric, that were linked to three USGS urban land use classes.

2.3. CAMx setup

CAMx v5.40 model (ENVIRON, 2011) was used to simulate dispersion phenomena and chemical processes at regional scale. CAMx provided the concentration fields for the outer domains and background contributions for the local domain, better detailed below. CAMx was setup using the same horizontal grid structure as for WRF. CAMx vertical grid was defined collapsing the 27 vertical layers used by WRF into 14 layers in CAMx but keeping identical the layers up to 1 km above ground level; in particular, the first layer thickness was up to about 25 m from the ground like the corresponding WRF layer. The model was run only for the three innermost domains of WRF (Italy, Po Valley, Milan area), adopting the same grid step but slightly reduced dimensions to remove boundary effects. Details on the computational grids are reported in Table S 1 of Supplementary materials section.

Homogenous gas phase reactions of nitrogen compounds and organic species were reproduced through CB05 mechanism (Yarwood et al., 2005). The aerosol scheme was based on two static modes (coarse and fine). Secondary inorganic compounds evolution was described by thermodynamic algorithm ISORROPIA (Nenes et al., 1998), while SOAP (ENVIRON, 2011) was used to describe secondary organic aerosol formation. Meteorological input data were provided by WRF and were completed by OMI satellite data (http://toms.gsfc.nasa.gov), including ozone vertical content and aerosol turbidity. Vertical turbulence coefficients (k_v) were computed using O'Bryan scheme (O'Brien, 1970), but adopting two different minimum k_v values for rural and urban areas, so to consider heat island phenomena and increased roughness of built areas.

Emissions were derived from inventory data at three different levels: European Monitoring and Evaluation Programme data (EMEP, http://www.ceip.at/emission-data-webdab/emissions-used-in-emep-models/) available over a regular grid of 50x50 km^2; ISPRA Italian national inventory data (http://www.sinanet.isprambiente.it/it/sia-ispra/inventaria/disaggregazione-dellinventario-nazionale-2010) which provides a disaggregation for province; regional inventories data based on INEMAR methodology (INEMAR – ARPA Lombardia, 2015) for the four administrative regions in the Po Valley, which provide detailed emissions data at municipality level. Each emission inventory was processed using the Sparse Matrix Operator for Kernel Emissions model (SMOKE v3.5) (UNC, 2013) in order to obtain the hourly time pattern of the emissions. Temporal disaggregation was

based on monthly, daily and hourly profiles deducted by CHIMERE model (INERIS, 2006) and EMEP model from Institute of Energy Economics and the Rational Use of Energy (IER) project named GENEMIS (Pernigotti et al., 2013).
In order to avoid the double counting of the emissions placed inside the local domain, the source apportionment algorithm PSAT (Yarwood, 2004) implemented into CAMx was used. PSAT allows keeping track of the contribution of different emission areas and source categories to the total pollutant concentration. For this application PSAT was setup to split the ambient concentrations resulting from the emissions of two Milan areas: innermost domain contribution ("local") and external domain contribution ("background"). The former contribution derives from the emissions belonging to the overlapping LSM-CTM urban domain, while the latter accounts for all the remaining sources, also including the CAMx parent domains. Therefore, in the context of this paper, "local" and "background" does not refer to the usual definition of the urban areas, but to the computational domains of the two modeling layers.
This approach allows avoiding double counting of emission sources preserving physical and chemical consistency between the two models, in a simpler way than other methods requiring more simulations and assumptions (Stocker et al., 2014).
Initial and boundary conditions were taken from MACC-II system (http://www.gmes-atmosphere.eu/services/aqac/) that provides 3D global concentrations fields.

2.4. AUSTAL2000 setup

AUSTAL2000 v2.6.9 release was used as LSM within the modelling chain. AUSTAL2000 computational domain almost exactly overlapped one CAMx cell, covering a 1.6x1.6 km^2 urban area, including the main square of Milan city center, with 20 m grid step size (Figure 2). The innermost domain is characterized by heterogeneous urban pattern: public parks (green area in the figure below) and road arches separate the densely built up area. Actually, the ring road is trafficked street during the all week-day. Based on the same emissions and meteorological parameters used by CAMx, AUSTAL2000 computed NO_X time series of concentrations generated by local sources enabling for the analysis of their spatial variability at high resolution within the urban domain. The vertical domain started from ground level up to 1500 m, adopting a variable-step grid: a 3m-step was used up to 60 m (i.e: twice the average height of the buildings), the top of the following three layers was set at 65 m, 100 m, 150 m, then a 100m-step was used from 200 m to 800 m and the top of the last three layers was set at 1000 m, 1200 m and 1500 m.

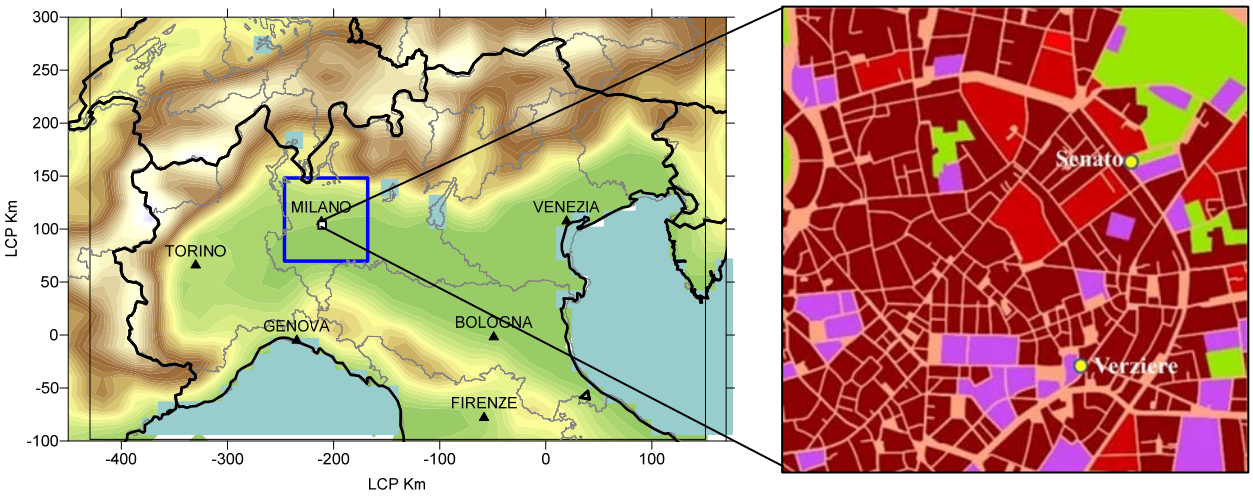

Figure 2. Overview of Milan area boundary (left panel). View of AUSTAL2000 urban computational domain (right panel). Yellow dots represent the air quality stations included within the urban domain used for validation. Green areas represent public parks.

Meteorological input variables for AUSTAL2000 (hourly data for Monin-Obukhov length, wind speed and direction) were provided by WRF and considered as representative of the non-disturbed flow; then the local wind field was calculated by the diagnostic wind field model TALdia, coupled with AUSTAL2000 and able to take into account the features of the urban built environment.
European land use atlas (http://www.eea.europa.eu/data-and-maps/data/urban-atlas), which provides information on the land cover composition according to the CORINE approach, was used to describe the presence of buildings in the urban domain. The cells covered at 99% by urban category land use, were considered as a building, with an assumed height of 30 meters based on the evidence of the average building height in Milan.
AUSTAL2000 used the same emission data as CAMx but with a more accurate spatial distribution that better mirrored the actual location of the sources and the release height. Namely, total NO_X emissions of the CAMx cell corresponding to the AUSTAL2000 urban domain were split among its cells based on proper 20x20 m^2 gridded information. According to CAMx emission data, NO_X emissions over the local domain were related only to domestic and commercial heating and to road traffic. Domestic heating emissions were equally split among all the cells associated to buildings in the urban domain, lacking specific information on the energetic system and performance of the real buildings. Each building was associated to a stack represented as a point source at the building rooftop height. Traffic emissions were dealt with as ground-level linear sources, allocated with high accuracy within the domain exploiting the full potential of LSM model. Total NO_X traffic emissions were proportionally split among all road arches in the local domain based on road network data provided by AMAT (http://www.amat-mi.it/it/documenti/dettaglio/16/). Emissions for each road have been computed as a weighted average of the total emissions within the local domain based on an aggregate street variable (ASV) given by the product of street length and vehicle number. AUSTAL2000 model operated considering NO_X as an inert species. However this limitation did not affect the results because of the very short atmospheric residence time within the local domain.

2.5. Hybrid modeling system output

HMS was applied to assess hourly NO_X concentration for the AUSTAL2000 computational domain showed in Figure 2. In the hybrid approach CAMx provided the background contribution, whilst AUSTAL2000 reproduced the hourly field concentration generated only by the sources active in the innermost urban domain; the final NO_X hourly concentration field at the Milan area domain was computed adding the local scale AUSTAL2000 concentration field to the CAMx background concentration. This approach avoided the double counting of local emissions that could occur when the LSM results for the local domain are simply superimposed to the regional scale results from CTM.
HMS results were compared with measurements at two air quality monitoring stations (Senato: 9,1974E, 45,4705N; Verziere: 9,1953E, 45,4633N) in the urban domain operated by the regional agency for environmental protection. Both stations are located in kerbside position near trafficked streets and Senato station is classified as an urban canyon environment. Figure S 2 in S.M. shows plan view of the two monitoring sites. In order to illustrate the local situation and micro-enviroments of both monitoring sites, the different impact of buildings on local scale winds is shown by the wind roses obtained by TALdia meteorological model for January 2010, reported in Figure S 3 in S.M. In particular, the screen effect of the building “west” of Verziere monitoring site (Figure S 4 – right), as well as the channeling effect of buildings along the city center ring road at Senato site (Figure S 4 – left) are clearly highlighted. However, because at these sites no wind measurements are available, TALdia results cannot be validated. Additionally, it was also possible

to compare the HMS results with those simply produced by the CTM as a result of both the emissions inside and outside the urban domain (stand-alone CAMx).
The statistical parameters for model performance assessment included the mean bias (MB), mean absolute error (MAE), root mean square error (RMSE), index of agreement (IOA) and the correlation coefficient (r). The explicit definition of each parameter is reported in the S.M. section.

3. Results and discussion

3.1. WRF performance evaluation

Meteorological fields were compared against surface observations proving that WRF was able to capture the temporal evolution of both the wind speed and direction over 2010. WRF Performance was evaluated considering the Po Valley and Milan area domain through two different observation networks: the World Meteorological Organization (WMO) and the Regional meteorological networks (ARPA). WRF provided similar performance for both networks; therefore, only the comparisons with ARPA data are shown in Figure 3 and Figure 4 for the Po valley and Milan area domain, respectively. Additional WRF performance results are available in the Table S 2 and Table S 3 of S.M. for both ARPA and WMO network.
Year 2010 was characterized by a normal rise of specific humidity (mixing ratio) with a peak in the summer period, as temperature trend. Occasionally quick decrease of temperature and mixing ratio were well captured by WRF over both domains during winter and summer months too. This is clearly proved by the values of the correlation index (Table S 2) showing values higher than 0.95 for both parameters and domains. Temperature over the Milan area domain was slightly overestimated over the whole year (BIAS = 0.67 deg), but the overall performance is better than the Po Valley domain, as stated by RMSE index, decreasing from 2.68 to 2.01. The observed annual wind speed distribution was correctly reproduced by WRF although a slight overprediction, higher for Milan area domain (BIAS=0.47 m/s) than Po Valley area (BIAS=0.3 m/s). Observed wind speed percentiles performed within Milan area domain were lower than wider domain, stressing critic situation for pollutants dispersion expected for Po Valley and urban domain.
Wind speed was constantly overpredicted over both domains but simulation for Milan area WRF showed an increased discrepancy in more windy conditions as shown by the 95^{th} percentile of the observed (2.67 m/s) and predicted (3.48 m/s) wind speed.

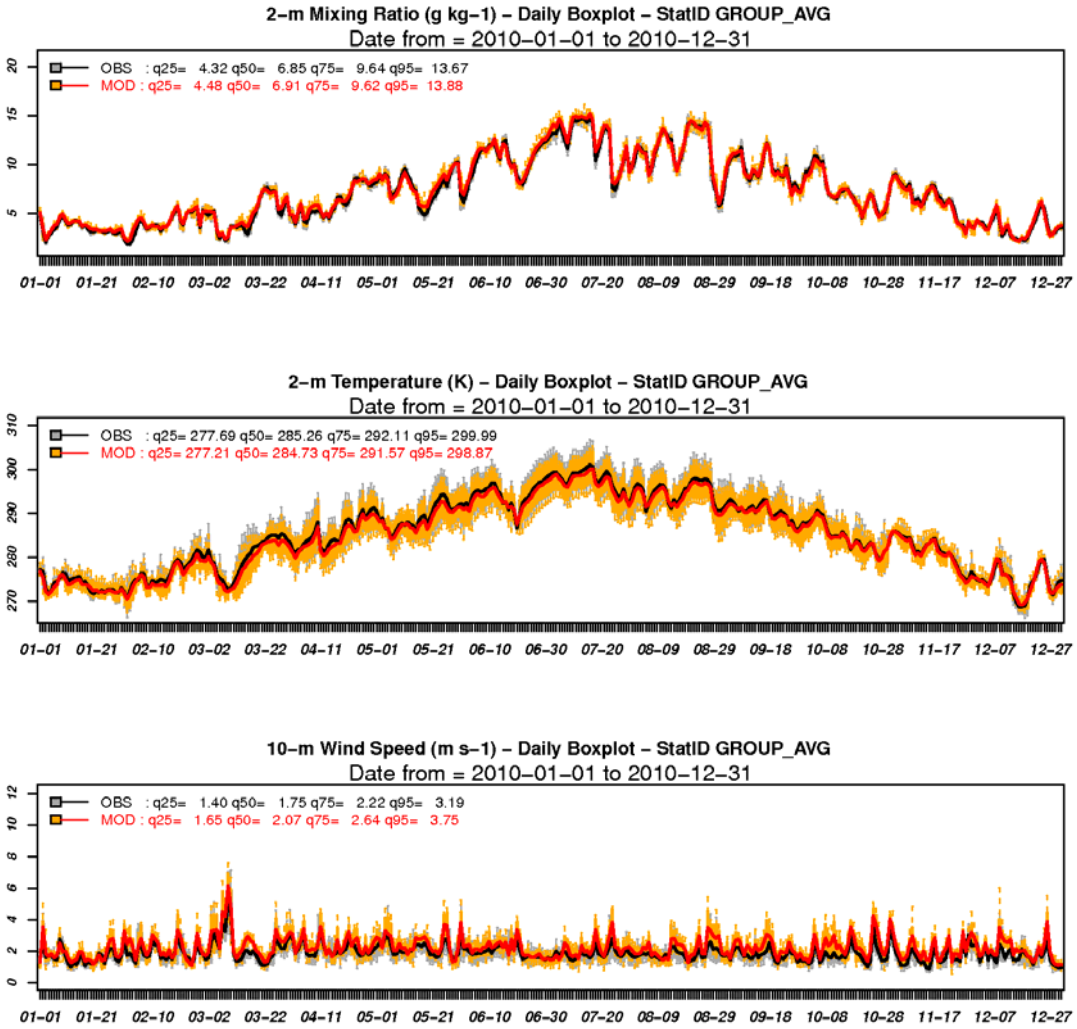

Figure 3. Time series of the box and whisker plots for the daily distribution of the observed (black/grey) and computed (red/orange) values of mixing ratio, temperature and wind speed at 170 ARPA sites, computed over the Po valley domain for 2010. Bars show the interquartile range (IR), lines the median values, dashed vertical bars the (25th – 1.5 · IR) and the (75th + 1.5 · IR) value. Values for the 25th, 50th, 75th, and 95th quantiles of the whole yearly time series are reported too.

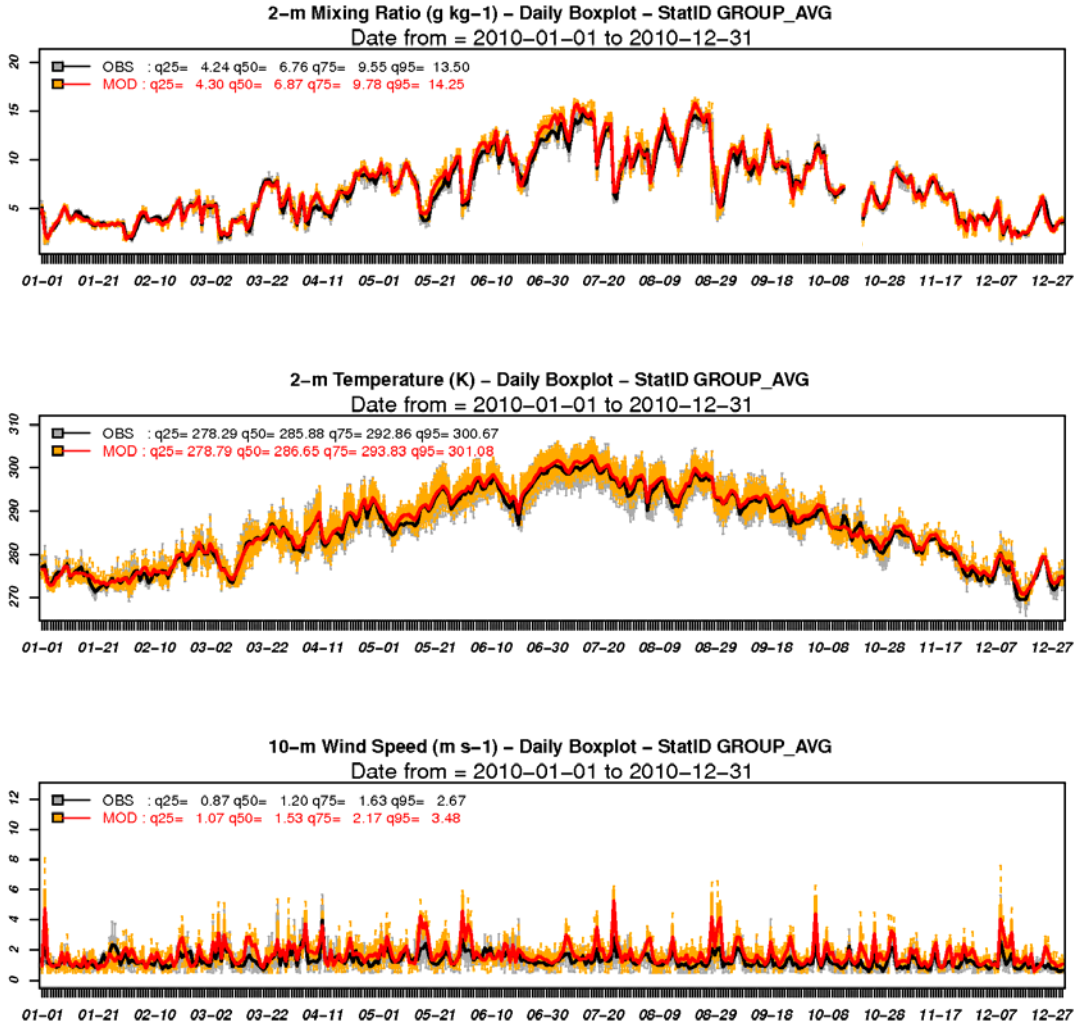

Figure 4. Time series of the box and whisker plots for the daily distribution of the observed (black/grey) and computed (red/orange) values of mixing ratio, temperature and wind speed at 15 ARPA sites (only 3 sites for wind speed), computed over the Milan area for 2010. Bars show the interquartile range (IR), lines the median values, dashed vertical bars (25th – 1.5 · IR) and the (75th + 1.5 · IR) value. Values for the 25th, 50th, 75th, and 95th quantiles of the whole yearly time series are reported too.

3.2. Stand-alone CAMx performance evaluation

CAMx performance was computed over both Po Valley and Milan area domains. CAMx should reproduce the atmospheric behavior of all main gaseous and aerosol pollutants, taking into account all relevant processes ought to be available in the code. According to the aim of the work, in this paper only results concerning NO_X concentration are presented and discussed.

Table 1 shows the comparison between statistical indicators over the two domains, considering only urban and suburban air quality monitoring stations. Measurements at 20 urban sites and 8 sub-urban sites were available for the Milan area and at 97 urban sites and 43 sub-urban sites, also including the previous ones for the whole Po Valley domain. Observed mean concentration increased from 30 ppbV to about 40 ppbV zooming from the whole Po Valley to the Milan area, due to the increasing strength of the anthropogenic emissions. Over both domains CAMx clearly underestimated the observed concentration, especially during the winter period, with an overall mean bias around 14 ppbV. As shown in Figure 5, regardless for the spatial resolution of the simulation, CAMx was able to reproduce the observed concentration for most of the summer months, but missing several of the

severe episodes that took place on winter months, particularly January and December which caused a low correlation index. Indeed, the difference between modelled and observed time series became larger and larger in the upper tail of the distribution, as pointed out by the values of the three quartiles and of the 95th percentile reported in Figure 5.

The origin of NO_X underestimation, mainly during the cold season, was not clearly identified, but it could be probably explained by the potential overestimation of the vertical mixing because, as stated in the previous paragraph, horizontal dispersion was well captured by WRF model. Wind direction also could be a reason for the NOx underestimation but the error showed in S.M. in the Figure S 5 over the Milan area was not so relevant and homogenously distributed for different wind speed. Thus at basin scale, the effect of the wind direction error on discrepancies between observations and model outputs was limited. Low wind speed, dry air and cold temperature that characterized principally the winter period in the Po valley, were often linked to strong inversion conditions with very low mixing heights, favoring pollutant accumulation, but direct measurements of mixing height were not available. However, focusing on peak events during the cold season, WRF slightly overestimated temperature and this could overestimate mixing layer height too. Similar performances are observed for the few rural stations available in the domain in S.M., in particular in Figure S 6 and Table S 4.

Additionally, it is worth noticing that CAMx provided the same performance for both the simulation domains, pointing out that the underestimation had not be ascribed to local scale effect (e.g. missing local sources), but to larger scale features not captured by the meteorological model.

Table 1. Comparison of stand-alone CAMx model performance for NO_X hourly concentrations computed for 2010 at urban and suburban AQ stations of Po Valley and Milan area domain.

	Po Valley		*Milan area*	
	Observations	Model	Observations	Model
Mean [ppbV]	29.7	14.9	39.4	26.5
Standard Deviation [ppbV]	35.1	17.5	46.4	24.0
Number Observations [-]	1173403		237587	
Correlation [-]	0.45		0.5	
Mean Bias [ppbV]	-14.8		-13	
Mean Error [ppbV]	19.5		23.2	
Index_of_Agreement [-]	0.56		0.6	
RMSE [ppbV]	34.7		42.3	

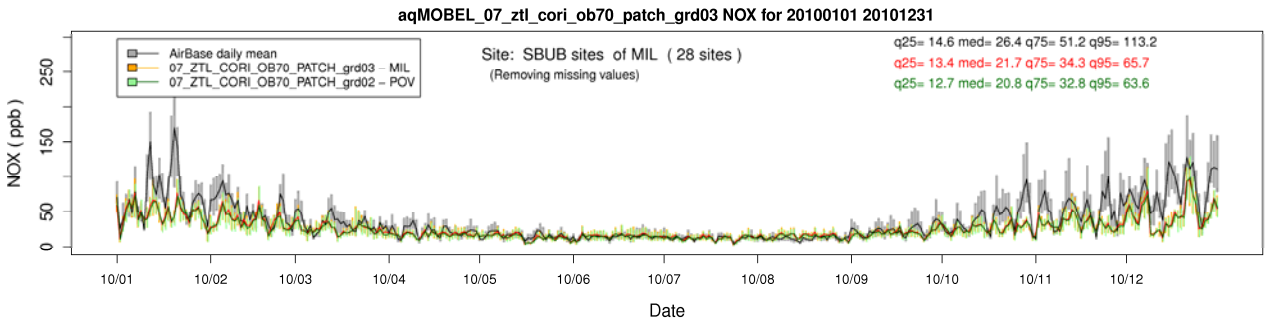

Figure 5. Time series of the box and whisker plots for the daily distribution of the observed (black/grey) and computed values of NO_X concentration (ppb) at Urban and Suburban monitoring sites of the Milan area domain for 2010. CAMx results at 5 km and 1.7 km resolution are displayed in red/orange and in green, respectively. Bars show the interquartile range, lines the median values. Values for the 25th, 50th, 75th, and 95th quantiles of the whole monthly time series are reported too.

3.3. CAMx and AUSTAL local concentration fields

AUSTAL2000 made possible the reconstruction of the urban structure of the city including buildings and all the obstacles that influence dispersion of pollutants. Figure 6 shows the NO_X spatial distribution over the local domain as ground-level mean concentration for 2010.

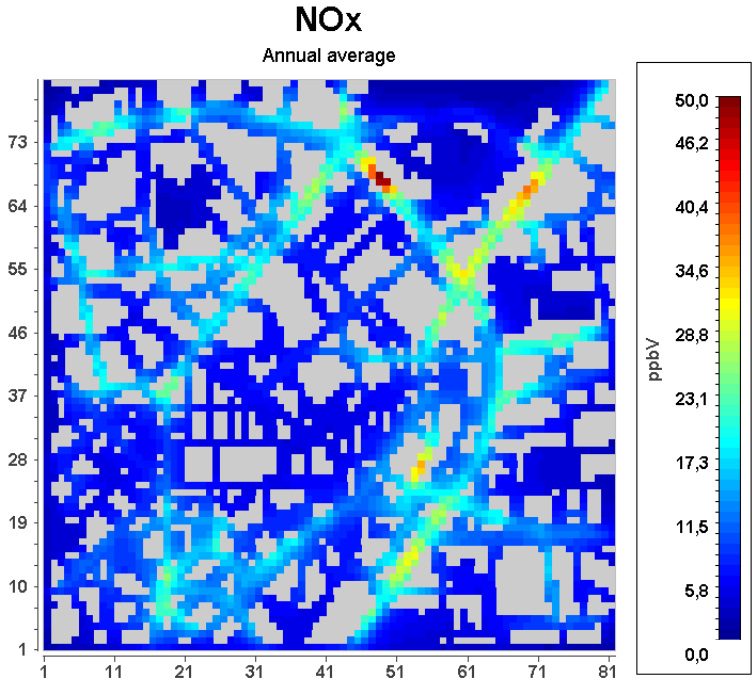

Figure 6. AUSTAL2000 NO_X mean concentration field for 2010 at ground level, computed as a vertical average along the first 24 meters (HMS_mean24m). Grey areas identify buildings.

Such a mean concentration field points out the effect of traffic sources on main roads of the area, responsible for NO_X levels as high as 40 ppbV near busy crossroads, as well as areas with lower levels, down to about 10 ppbV, far from busy streets. This result highlights the LSM capability to reproduce the strong spatial variability of pollutants within urban areas, that cannot be captured by a CTM alone, that over the same area can provide only one mean concentration value.

An interesting feature of our HMS is that the LSM output can be compared with the CTM local contribution (CAMx local), obtained by PSAT application, because both of them are produced by the same emissions sources. To this purpose, AUSTAL2000 vertical concentration profiles were averaged within the first 24 meters, in order to make them comparable to CAMx first layer output (up to around 25 meters). Then, in order to preserve LSM variability, the CAMx mean local concentrations were compared to the statistical distribution of the AUSTAL2000 concentrations, excluding those cells representing a building or general obstacles.

Figure 7 shows the comparison between the mean estimations from CAMx and the box plots representing the distribution of daily mean NO_X concentrations over all the urban domain from AUSTAL2000. In order to highlight the higher concentrations performed by AUSTAL2000, the scatter plot and the main statistical parameters from the two different local contributions were showed in Figure S 7 in S.M, based on the median value of AUSTAL2000 daily concentrations and CAMx local contribution.

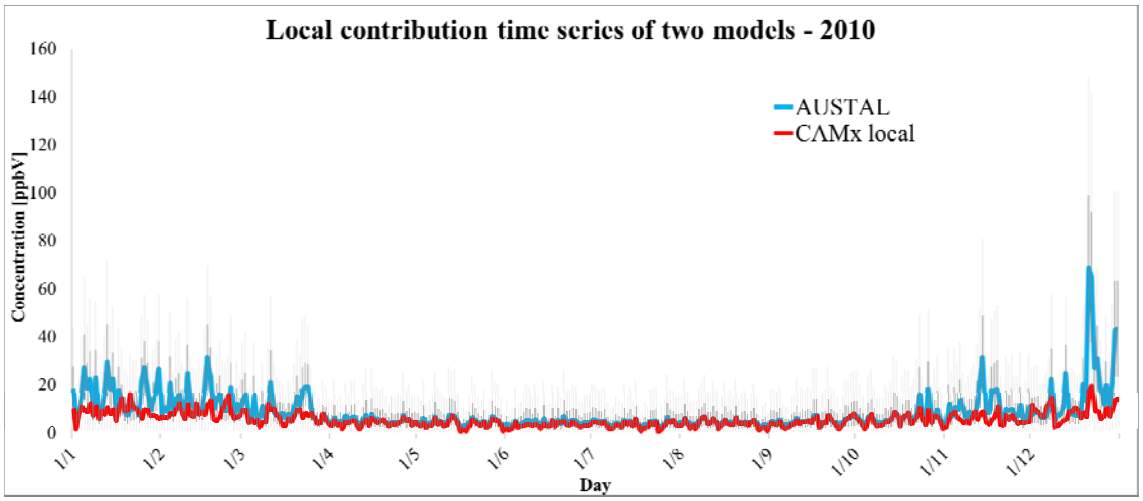

Figure 7. Comparison between NO_X daily concentrations for the urban domain computed by CAMx local (red line) and by AUSTAL2000. The latter is expressed as statistical distribution, with the blue line representing the median value of the spatial distribution, the blue box limits the 25th and 75th percentile of the distribution and the grey line the 5th and 95th percentile.

The two models were driven by the same meteorological input and the same emission data but based on very different modelling approaches (CAMx is an eulerian model while AUSTAL2000 follows a lagrangian approach). CAMx local concentrations mostly ranged between 0 and 20 ppbV while AUSTAL2000 showed several peaks ranging between 10 and 70 ppbV. Nevertheless the models showed a rather good agreement in some periods, especially when the estimated contribution from "local sources" was below 10 ppbV (e.g.: between April and October). Conversely, in some other periods the whole distribution of AUSTAL2000 concentrations was higher than the CAMx local value, though both the models tended to reproduce the same time pattern. Other than to the different modeling approach, the discrepancy between the models can be related to different sensitivity to meteorological data.

The effect of atmospheric stability on model performance was highlighted by the comparison between the daily pattern of the computed "local sources" contributions (Figure 8) for a winter a summer month. In January, differences between models are related to nighttime hours, when AUSTAL2000 showed a more pronounced temporal variability than CAMx with two peaks corresponding to morning and late afternoon rush hours. Differently, CAMx computed a slighter growth of concentrations on morning and evening rush hours and a flatter concentration time pattern over the whole day. Conversely, on daytime hours model results were very similar, but with CAMx mean values slightly higher. The model outputs largely differed on late evening hours, when the stratification of the atmosphere, more relevant for the LSM, drove AUSTAL2000 to emphasize backlog conditions and consequently NO_X concentration levels.

An additional analysis of the influence of winter meteorological conditions on concentration levels computed at Verziere and Senato site, the two air quality monitoring sites also used for model performance evaluation, is shown in Figure S 8. At both sites, the most part of hourly concentration events when the local sources' contribution estimated by AUSTAL2000 exceeded 50 ppbV occurred under "critical conditions", associated with wind speed lower than 1.5 m/s and Monin-Obhukov length in the 0.1 - 50 m range, thus representing stable atmospheric conditions.

The combined analysis of Figure 8 and Figure S 8 points out that the "critical conditions" were prevailing during nighttime hours, when the absence of solar radiation favored the development of more stagnant conditions.

In June modeled concentrations are lower than winter for both models, as expected. CAMx and AUSTAL2000 showed a similar behavior during nighttime hours, while CAMx was lower than AUSTAL2000 during daytime. This results points out that CAMx is characterized by an enhanced vertical mixing during daytime hours of the warm season (Lonati et al, 2010).

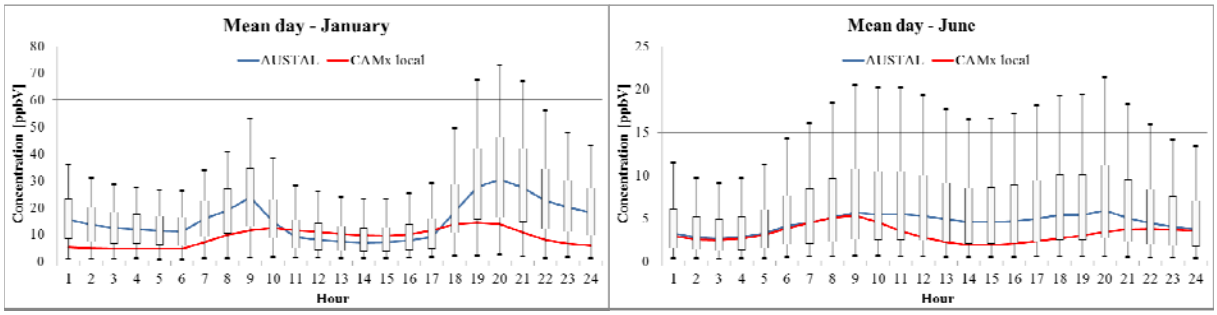

Figure 8. NO_X January (left) and June (right) mean day concentration. Red line represents CAMx local estimation. Blue line represents the median of AUSTAL2000 spatial distribution of the mean day concentrations, while the box's limits indicate 25th and 75th percentile and the vertical lines link the 5th and 95th percentile.

3.4. Hybrid modeling system performance

Adding AUSTAL2000 output to the background concentration computed by CAMx, it was possible to obtain the HMS estimation of the total NO_X concentration, without any double counting of local sources. HMS output was compared with observations as well as with the results of the stand-alone CAMx simulation. The definition of the HMS "total" NO_X concentration requires additional assumptions. Indeed, AUSTAL2000 results are available over a 3m-stepped vertical profile, observed values generally refers to 2 m above ground level, while CAMx concentration represents the mean value for the first vertical layer. For this reason, at a first stage, the model performance evaluation was based on two different definition of the LSM concentration contribution: AUSTAL2000 contribution at 3 meters from the ground (HMS_3m) was used for comparison with measurements, which are sampled at a similar height; AUSTAL2000 average contribution of first 24 meters (HMS_mean24m) was used for comparison with CAMx estimation. In Figure 9 the measured time series (black line), stand-alone CAMx estimate (red line) and HMS values made by background contribution (blue area) and AUSTAL2000 contribution (green area) are plotted. The analysis referred to Verziere and Senato site, the two only monitoring sites available within the local domain.

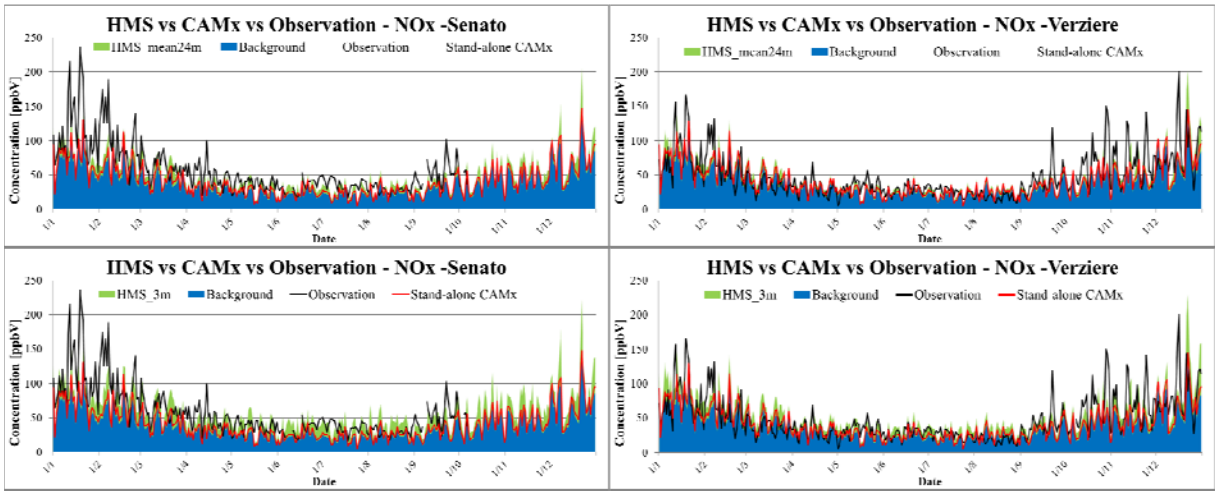

Figure 9. Comparison of daily mean NO_X concentrations observed and computed by the HMS, according to both definition, and stand-alone CAMx for Senato (left column) and Verziere site (right column). HMS concentration

is obtained superimposing CAMx background concentration (in blue) with AUSTAL2000 local contribution (in green). AUSTAL2000 contribution in HMS time series is HMS_3m in top graphs and HMS_mean24m in bottom graphs. Stand-alone CAMx results are in red.

The first relevant finding stemming from Figure 9 is that, in most cases, the total HMS concentration was mainly due to the background contribution, thus depending on the sources placed outside the AUSTAL2000 local domain. The mean modeled contributions are summarized in Table 2, showing a background concentration around 36 ppbV. Local contributions at Senato site ranged between 4 ppbV for CAMx local up to 21 ppbV with AUSTAL2000 at 3m and between 4.9 and 18.1 at Verziere site. This result implies that, first of all, the reconstruction of air quality levels within urban areas, even in an intensely emitting area like Milan city center, requires a modeling approach able to take into account the influence of sources placed over the whole urban context.
Table 3 reports the main statistical parameters summarizing model performance for both HMS outputs and for stand-alone CAMx output.
Both the observed annual mean concentration and the standard deviation of hourly concentrations at Senato site were higher than at Verziere site. The reason is probably related to local features of urban morphology as shown in Figure S 2 but also to the traffic load on the two streets. Actually, Verziere street is a secondary road, less trafficked compared to Senato street, that is a stretch of the city center ring road with the aspect of an urban canyon. Therefore, in addiction to high local NOx emissions, there are also buildings surrounding Senato monitoring station, that emphasize backlog conditions rather than at Verziere site where, moreover, the wider open area favors the dispersion of local emissions. Neither stand-alone CAMx nor the HMS were able to capture this feature. Indeed all the model configurations showed increasing concentrations from stand-alone CAMx to HMS_3m, but without relevant differences between the two sites. This suggests that both the difference in urban morphology and in the emission load were not well captured by the HMS.
At both sites the statistical indexes showed a general underestimation for CAMx stand-alone (negative bias: -20.8 at Senato, -6.5 at Verziere), but improved with HMS application. Bias decreased of almost 8 ppbV at Senato site using HMS with AUSTAL2000 vertical average and of more than 16 ppbV with AUSTAL2000 at 3m, anyway still remaining negative (-4.4 ppbV); at Verziere site bias was still negative, reaching a value of -0.1 ppbV with HMS_mean24m, but became positive with HMS_3m (6.7 ppbV). Correlation index showed a slight worsening for both HMS options with respect to CAMx: from 0.84 for CAMx down to 0.78-0.81 for HMS at Senato site, from 0.73 down to 0.71-0.72 at Verziere site. The opposite trend of bias and correlation index, as well as of index of agreement, points out that: i) the higher concentrations produced by HMS with respect to stand-alone CAMx reduced, on the average, the model underestimation; ii) the presence of several peaks produced by AUSTAL2000 during nighttime stable conditions worsened the reproduction of the temporal evolution of NO_X concentrations.
The combined effect of both these aspects on model performance is supported by joint evaluation of the Index of agreement (IOA) and Root Mean Square Error (RMSE). Actually, with respect to stand-alone CAMx, the IOA computed for HMS options remained substantially unchanged at Senato site, where the worsening in correlation was compensated by the clear improvement in bias and a slight one in RMSE, especially for HMS_mean24m approach; differently at Verziere site IOA and RMSE showed a degraded performance, especially for HMS_3m.
In contrast with the improvements obtained for the BIAS, HMS_3m approach produced worst performance at both sites when IOA and CORR are considered. Conversely, HMS_mean24m shows less relevant improvements but extended to all the statistical performance indicators.
This aspect can be explained by the significant backlog capability of LSM at ground-level during stable conditions (night-time), confirming the HMS_mean24m as best solution between the two approaches.

Table 2. Comparison among the modelled contributions to the yearly mean concentration and corresponding standard deviations.

Statistical Parameters [ppbV]	*Milano Senato*				*Milano Verziere*			
	CAMx Background	*AUSTAL2000 24m*	*AUSTAL2000 3m*	*CAMx local*	*CAMx Background*	*AUSTAL2000 24m*	*AUSTAL2000 3m*	*CAMx local*
Mean	36.7	13.4	21.4	4.2	36,3	11.3	18.1	4.9
St. Dev	21.2	14.9	20.6	3.5	20.8	13.4	18	4

Table 3. Statistical parameters of HMS and CAMx model performance at Senato and Verziere site.

Statistical Parameters	*Milano Senato*				*Milano Verziere*			
	Observ.	*HMS_mean24m*	*HMS_3m*	*CAMx stand-alone*	*Observ.*	*HMS_mean24m*	*HMS_3m*	*CAMx stand-alone*
Mean [ppb]	58.1	50.1	58.1	40.9	47.9	47.6	54.4	41.2
St. Dev. [ppb]	37.1	27.3	29.5	23.3	31.5	27.6	30.2	23.3
BIAS [ppb]		-12.2	-4.4	-20.8		-0.1	6.7	-6.5
MAE [ppb]		26.5	27.2	28.1		24.9	27.1	23.9
IOA [-]		0.92	0.92	0.93		0.84	0.81	0.86
RMSE [ppb]		40.9	41.6	42.2		38.1	40.8	36.1
CORR [-]		0.81	0.78	0.84		0.72	0.71	0.73

The analysis of the whole distribution of measured and modelled NO_X time series showed that all CAMx stand-alone distributions systematically underpredicted the measurements at both sites, especially at Senato site. (Figure 10 and Figure S 1 in S.M.) This behavior improved with the introduction of the HMS, but there were still relevant discrepancies, particularly for the highest percentiles. A better agreement with modelled data was observed at Verziere site, particularly for HMS_mean24m data. This confirms that HMS was able to add properly the local scale magnitude of NO_X concentrations to background contribution at this site, but not always to reproduce their temporal variability as confirmed by statistical indexes shown previously. At this site we could also observe a very good agreement for stand-alone CAMx output up to the 50th percentile while a systematic underestimation for Senato site, even though HMS_mean24m application, confirms that some specific local scale features were not captured by our modeling approach. Indeed, we already pointed out that highest observed concentrations took place during very stable conditions when local scale accumulation processes, that cannot be captured by CAMx, were prevailing.

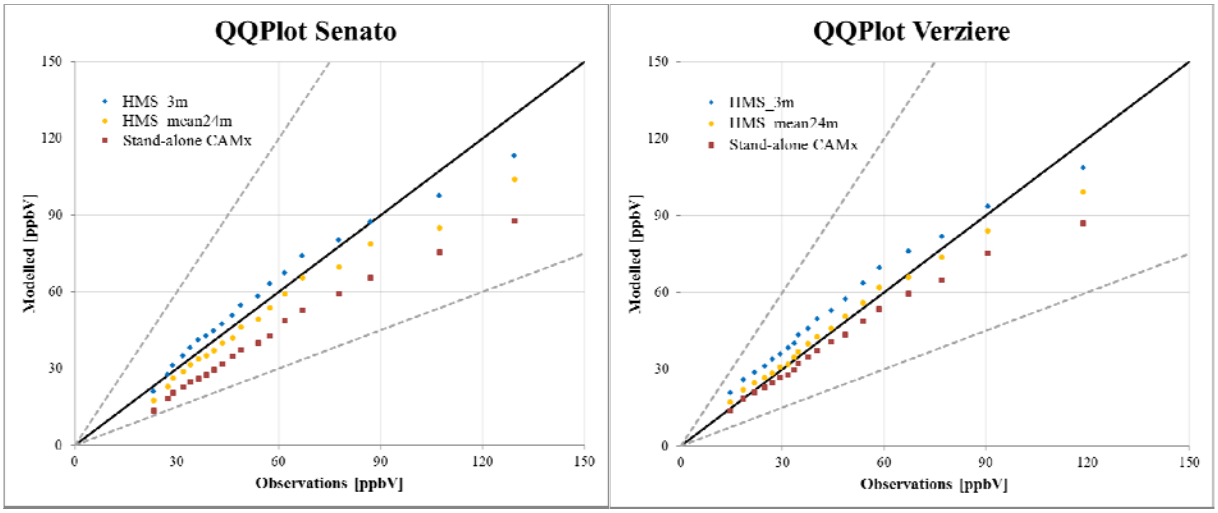

Figure 10. Quantile-Quantile plot of the observed and modelled NO_X daily concentrations at Senato (left) and Verziere (right) site, starting from 5th percentile up to 95th percentile with a step of 0.05.

Although the highest percentiles underestimation persists after HMS introduction, the overall improvements will allow to capture a better level of exposure to pollutants of people living in high-density urban areas, particularly at hot spot sites, generally missed by larger scale model.

A further analysis of model performance was carried out considering the average weekly pattern and the mean day of modelled and observed NO_X concentrations (Figure 11). The "day of the week" analysis shows that both HMS and stand-alone CAMx were able to capture the decreasing trend between workdays and weekends, especially in January, while failing in reproducing the day-by-day variability observed also during workdays. The origin of such variability, especially observed at Senato site, was not clearly identified and could not be properly reproduced with the current approach for emission processing, that used the same time pattern for all weekdays from Monday to Friday. The day-by-day variability as well as the absolute values of concentrations were quite well reconstructed during the summer month (June), especially at Verziere site that was not affected by morning rush hour peaks as at Senato site.

Figure 11 shows a negative bias at Senato site for January, across all weekdays. The discrepancy was mainly related to the strong underestimation of the morning peak and, as a consequence, of the ensuing daytime concentrations, as clearly pointed out by the mean day analysis in Figure 12. Other than to the emission pattern, the systematic under prediction of NO_X at Senato site, clear also during June, can be partly associated with an incorrect definition of the site's features as discussed before (e.g. street canyon character), that could not be captured by our modeling approach.

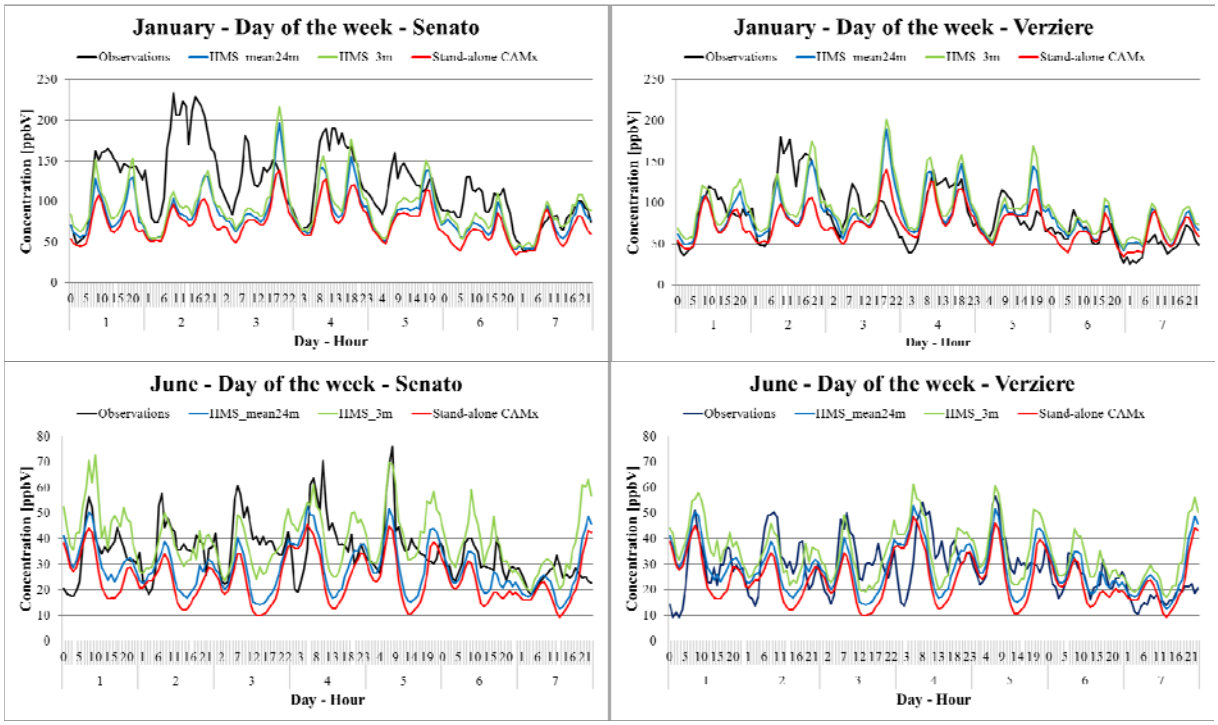

Figure 11. Day of the week for January (top) and June (bottom) NO_X concentrations at Senato (left) and Verziere (right) measurement site. Black line represents measure, red line indicates stand-alone CAMx concentrations, while green and blue line show HMS results. Day of the week ranges from Monday (1) to Sunday (7).

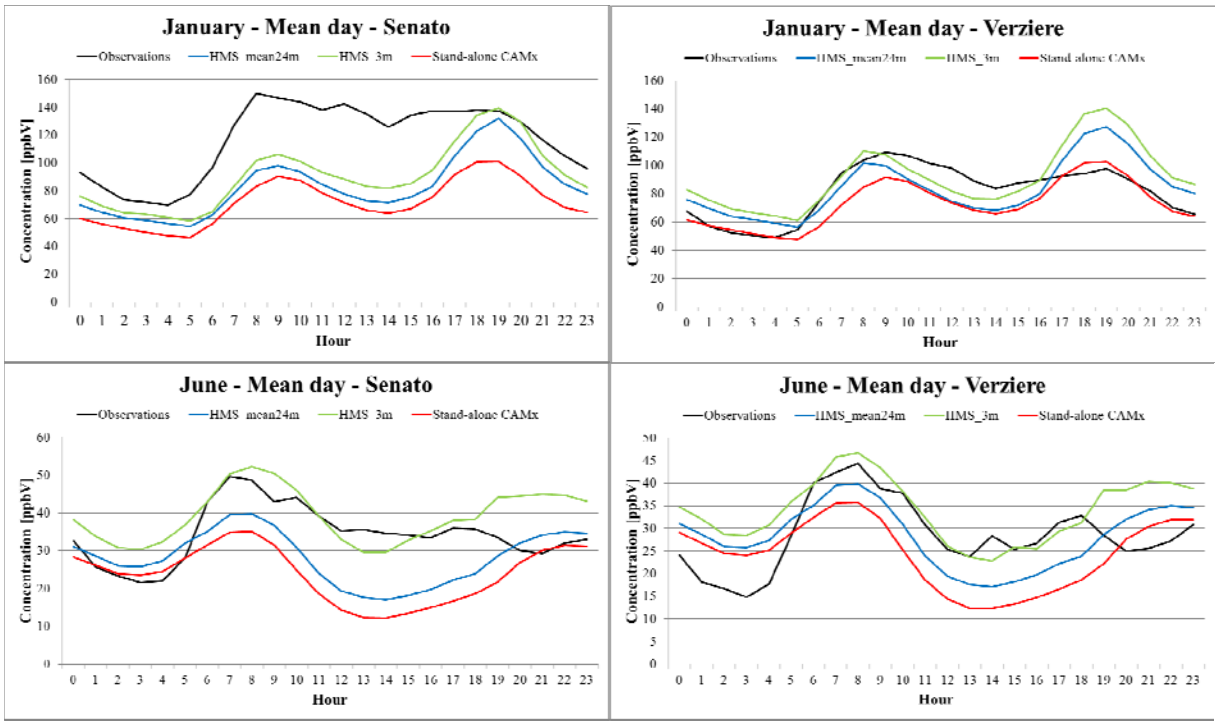

Figure 12. Mean day for January (top) and June (bottom) NO_X concentrations at Senato (left) and Verziere (right) measurement site. Black line represents measure, red line indicates stand-alone CAMx concentrations, while green and blue line show HMS results. Day of the week ranges from Monday (1) to Sunday (7).

Notwithstanding the day-by-day temporal variability not exactly reconstructed, the HMS (mean24m and 3m approach) results showed in Figure 12 confirmed that the average day-time variability modeled was not much different from observed concentrations, especially during the summer period when thermal and mechanical turbulence phenomena were more pronounced than in winter time. In particular, the magnitude of NOx concentrations observed in the winter (from 60 ppbV to 100 ppbV) and summer period (from 15 ppbV to 40 ppbV) was correctly reproduced.

However, the daily pattern was better reconstructed in the summer period than in the cold season. Indeed, traffic modulation and atmospheric conditions could influence significantly NOx concentrations during the hours of the day but CAMx stand-alone and especially HMS reproduce satisfactorily the morning and evening peak, moreover during summer months. Mechanical and relevant thermal turbulence during the warm season caused a lower evening peak, even though traffic modulation was similar to the cold season. This aspect was considered by both models (CAMx stand-alone and HMS).

In particular, at Verziere site model outputs showed the smallest bias (Table 2), with the observed concentrations rather well captured, by HMS_mean24m on both summer and winter months.

Actually, the main discrepancy was related to the overestimation of the evening peak in January, and to a lesser extent in June, on both workdays and weekends, even up to about 30 ppbV.

The consistent over prediction suggests either a not good agreement between modelled and real modulation of traffic emissions or a too strong decrease of vertical turbulence and mixing in the late afternoon. This latter phenomenon has been already highlighted by previous studies (Kim et al., 2015) and is related to the difficulty of meteorological model in taking into account the contribution of anthropogenic heating to energy balance within urban areas.

CAMx stand-alone and HMS approaches resulted in solutions regarding concentration levels somewhat different but temporal variability as shown in Figure 11 and Figure 12 was not affect by the two methods. This aspect suggests that horizontal resolution as well as modelling method could either increase or decrease the backlog capability of the models, but they are less influent on temporal evolution. Consequently, NOx temporal variability depends on emission temporal

modulation and overall meteorological parameters, which remains unchanged between the two approaches.

Finally, as for as the "double counting" is concerned, results reported in Table 2 for the annual mean concentration and the inspection of the daily pattern of the contributions computed by CAMx and AUSTAL2000 at the two monitoring sites (Figure 13) showed that the local sources' contributions could not be considered negligible. In particular, the CAMx local contribution (i.e. the potential "double counting") was in the 5%-15% range of the daily mean concentration considering both sites and months. Thus, correctly the CAMx local contribution must be excluded from HMS outcome to have a more accurate model estimate. AUSTAL contribution was in the 15%-25% range for January while during June the range increased up to 30% as daily average.

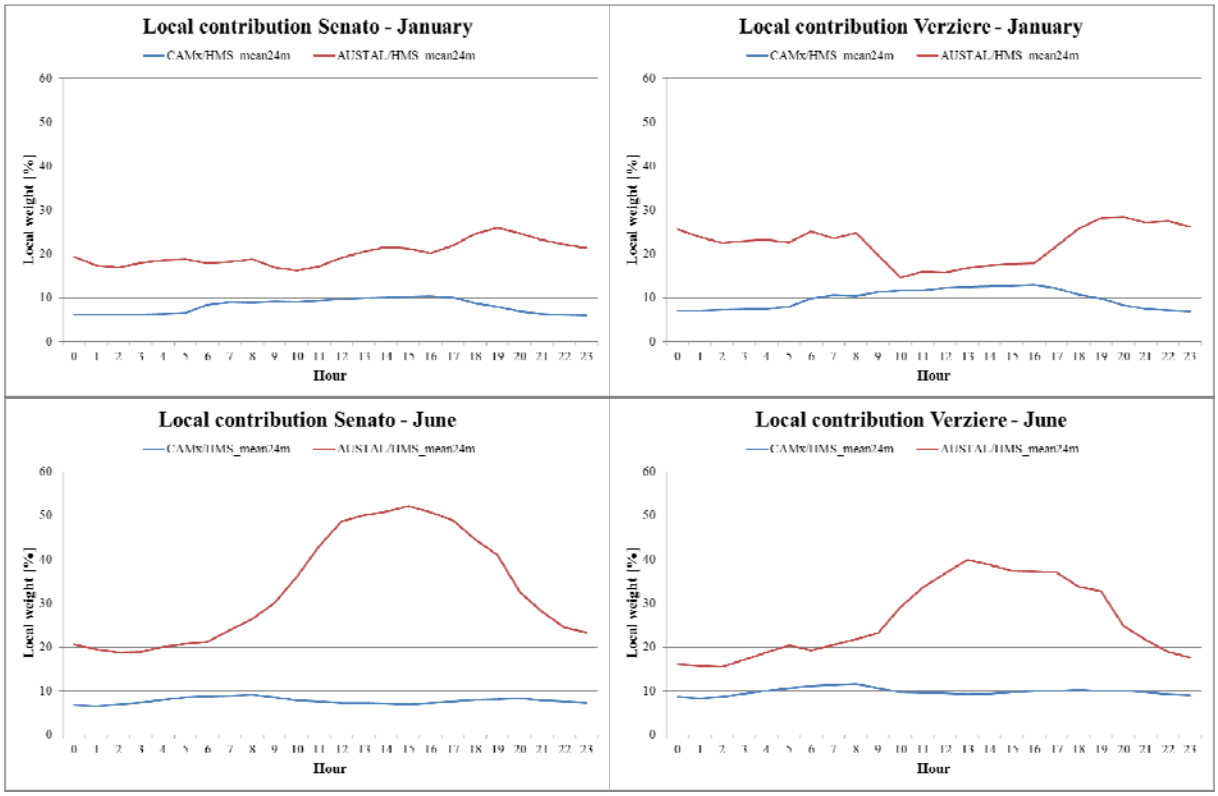

Figure 13. Daily pattern of the percentage ratio between estimated local contributions and HMS_24m daily mean concentration, computed for CAMx local (blue) and AUSTAL2000 (red) at Senato (left) and Verziere (right) site for January (top) and June (bottom).

4. Conclusions

A hybrid modeling system (HMS) was developed to provide hourly concentrations at the urban local scale. In this work the HMS was applied over a set of nested domains, the innermost covering a 1.6x1.6 km^2 area in Milan city center with 20 m grid step size. HMS is based on the combination of a meteorological model (WRF), a CTM eulerian model (CAMx), which computes concentration levels over the regional domains, and a lagrangian dispersion model (AUSTAL2000), which computes dispersion phenomena and relative concentrations, due to road traffic and domestic heating within the urban area. A source apportionment algorithm PSAT (Yarwood et al., 2008), is also included in the HMS in order to avoid the double counting of local emissions. PSAT is able to track contribution of different emission areas or source categories. In this application we split the NOx concentration level in two Milan emission areas' contribution: innermost domain contribution

("local") and external domain contribution ("background"). These two terms refer respectively to emission sources located within the innermost domain and to all remaining sources outside. Limitedly to this application "local" and "background" does not refer to the usual definition of the urban areas, while to the computational domains of the two modeling layers. The performance of the model components of the HMS was thoroughly evaluated for both meteorology and air quality reconstruction at the basin and local scale.

WRF captured the overall evolution of the main meteorological features, but failing in reproducing some very stagnant situations, thus influencing the subsequent performance of regional scale model CAMx. Indeed, CAMx was able to reproduce the spatial and temporal evolution of NO_X concentration over the whole regional and Milan area domain, with the exception of two severe episodes, characterized by observed concentrations higher than 100 ppb.

The local scale model AUSTAL2000 provided high-resolution concentration fields that sensibly mirrored the road and traffic pattern in the innermost urban domain. In spite of the different modeling approach, the local contributions estimated by CAMx and AUSTAL2000 were in good agreement, especially during daytime in the summer period when stronger dispersion conditions, due to increasing of height mixing layer, generate more homogenous concentrations over the first vertical layers. Conversely, AUSTAL2000 resulted in higher concentration levels on night hours due to pronounced backlog situations corresponding to atmospheric stratification phenomena.

According to the HMS the background contribution accounted on the average for about 70-75% of the computed concentration levels in the local domain, with the contribution of the local emission sources higher than the background only on particular events, mostly during atmospheric stability episodes (low wind speed and positive Monin-Obukhov length). This result, stating that NO_X concentration levels within the inner part of the urban area could be mostly influenced by the contribution of sources outside the local domain, confirmed that in Milan the whole urban area as well as the outside background areas play a key role on air quality and that strictly local policies on urban emission sources could have a limited and indecisive effect. However, this finding could be partially biased by model underestimation of the observed concentration.

In spite of the interesting additional pieces of information provided by HMS output about local scale modelling, namely concerning the detailed reconstruction of the spatial variability of NO_X concentration, the overall performance of the HMS did not provide remarkable improvements with respect to stand-alone CAMx. Model validation relied on hourly NO_X data collected for 2010 at the two only monitoring sites in the innermost simulation domain. Actually, with respect to stand-alone CAMx the HMS results were characterized by a smaller average bias as well as by a lower correlation, due to the concentration peaks produced by AUSTAL2000 during nighttime stable conditions that worsened the reproduction of the temporal evolution of NO_X concentrations. Vertical averaging of HMS output data provided a slightly more robust performance, as averaging along the first atmospheric layers reduced the effect of the overestimated influence of stable and stagnant atmospheric conditions.

The HMS provided rather similar results at both measuring sites, while observed values were clearly different, suggesting that some local scale features (e.g. the canyon effect at one site) still remain not correctly taken into account by the model or that the emission spatialization criteria, especially those from road traffic, need further improvement. Additionally, the analysis of the mean day concentrations highlighted that the HMS provided higher concentrations during evening hours. Such systematic over prediction suggests either a not good agreement between the time modulation of modelled and real world emission or a too strong decrease of vertical turbulence in the late afternoon related to the difficulty of the meteorological model in taking into account the contribution of anthropogenic heating to energy balance within the urban area. However, a first important outcome of the work is that some of the most relevant discrepancies between modeled and observed concentrations were not related to the horizontal resolution of the dispersion models, but to larger scale meteorological features not captured by the meteorological model. Secondly,

HMS output reduces the bias with observed NOx concentrations still keeping unaltered the time patterns (daily, weekly, monthly) of the CAMx model.
We have demonstrated that this hybrid approach for the prediction of pollutant concentrations in urban areas is promising, even though the performance of the HMS showed some limitations, partially due to some approximations in the local scale input data. Such limitations concerns, among others: the fixed height of the buildings, the width of the streets in relation to the grid step size, the domestic heating emissions partitioning, the split of traffic emission among the arches of the road network and to the value of the urban mixing layer height constrained by inherent model assumptions (Federal Ministry for Environment, 2002). In conclusion, the highly-resolved spatial and temporal scale of the HMS output can be used for refining human exposure and health impact assessment as well as for the assessment of the impact of energy and traffic policies on air quality at the regional and local scale.
Future work will also consider other pollutants, like particulate matter, a wider local domain in order to extent it to the entire urban area, and facing the abovementioned issues related to the input data for the local scale model.

5. Acknowledgements

This work has been financed by the Research Fund for the Italian Electrical System under the Contract Agreement between RSE S.p.A. and the Ministry of Economic Development - General Directorate for Nuclear Energy, Renewable Energy and Energy Efficiency in compliance with the Decree of March 8, 2006. The authors would like also to acknowledge ARPA Lombardia for air quality and meteorological observations data, necessary to evaluate HMS and the models which composed it.

6. References

Batterman, S., Chambliss, S., Isakov, V., 2014. Spatial resolution requirements for traffic-related air pollutant exposure evaluations. Atmospheric Environment 94, 518-528.

Beevers, S.D., Kitwiroon, N., Williams, M.L., Carslaw, D.C., 2012. One way coupling of CMAQ and a road source dispersion model for fine scale air pollution predictions. Atmospheric Environment 59, 47-58.

Chen, F., Dudhia, J., 2001. Coupling an advanced land-surface/hydrology model with the Penn State/NCAR MM5 modelling system. Part I: model description and implementation. Monthly Weather Review 129, 167-196.

Denby, B., Cassiani, M., de Smet, P., de Leeuw, F., Horálek, J., 2011. Sub-grid variability and its impact on European wide air quality exposure assessment. Atmospheric Environment 45, 4220-4229.

EEA, 2015. EEA technical report 1. No 1/2006. Air pollution at street level in European cities. Available at: http://www.eea.europa.eu/publications/technical_report_2006_1. (accessed 17.06.15).

ENVIRON, 2011. CAMx (Comprehensive Air Quality Model with extensions) User's Guide Version 5.4. ENVIRON International Corporation, Novato, CA.

Federal Ministry of Environment, Nature Conservation and Nuclear Safety, 2002: Technical instructions on air quality control – TA Luft, Germany

731 Grell, G.A., Devenyi D., 2002: A generalized approach to parameterizing convection combining
732 ensemble and data assimilation techniques. Geophys. Res. Lett., 29(14), Article 1693.
733 Kim Y., Sartelet K., Raut J.C., Chazette P., Influence of an urban canopy model and PBL schemes
734 on vertical mixing for air quality modeling over Greater Paris, Atmospheric Environment, Volume
735 107, April 2015, Pages 289-306, ISSN 1352-2310,
736 http://dx.doi.org/10.1016/j.atmosenv.2015.02.011.
737 Hellison, R.B., Greaves, S. P., Hensher, D.A., 2013. Five years of London's low emission zone:
738 Effects on vehicle fleet composition and air quality. Transportation Research Part D 23, 25-33.
739 Hong, S.-Y., Noh Y., Dudhia J., 2006: A new vertical diffusion package with an explicit treatment
740 of entrainment processes. Mon. Wea. Rev., 134, 2318–2341.
741 Iacono, M.J., Delamere, J.S., Mlawer E.J., Shephard M.W., Clough S.A., Collins W.D., 2008:
742 Radiative forcing by long-lived greenhouse gases: Calculations with the AER radiative transfer
743 models, J. Geophys. Res., 113, D13103.
744 INEMAR - Arpa Lombardia (2015), INEMAR, Emission Inventory: 2012 emission in Region
745 Lombardy - public review. ARPA Lombardia Settore Aria. Available at: http://www.inemar.eu/
746 INERIS, 2006. Documentation of the chemistry-transport model CHIMERE [version V200606A].
747 Available at: http://euler.lmd.polytechnique.fr/chimere/
748 Isakov, V., Arunachalam, S., Batterman, S., Bereznicki, S., Burke, J., Dionisio, K., Garcia, V.,
749 Heist, D., Perry, S., Snyder, M., Vette, A., 2014. Air quality modeling in support of the near-road
750 exposures and effects of urban air pollutants study (NEXUS). International Journal of
751 Environmental Research and Public Health 11, 8777-8793.
752 Isakov, V., Irwin J.S., Ching J., 2007. Using CMAQ for exposure modelling and characterizing the
753 subgrid variability for exposure estimates. Journal of applied meteorology and climatology 46,
754 1354-1371.
755 Isakov, V., Lobdell, D.T., Palma, T., Rosenbaum, A., Özkaynak, H., 2009. Combining regional- and
756 local-scale air quality models with exposure models for use in environmental health studies.
757 Journal of the Air & Waste Management Association 59, 461-472.
758 Janicke Consulting, 2014. AUSTAL2000. Program description of Version 2.6, 2014-02-24.
759 Technical report. Federal Environmetal Agency, Janicke Consuluting, Germany.
760 Lefebvre, W., Van Poppel, M., Maiheu, B., Janssen, S., Dons, E., 2013. Evaluation of the RIO-
761 IFDM-street canyon model chain. Atmospheric Environment 77, 325-337.
762 Lefebvre, W., Vercauteren, J., Schrooten, L., Janssen, S., Degraeuwe, B., Maenhaut, W., de
763 Vlieger, I., Vankerkom, J., Cosemans, G., Mensink, C., Veldeman, N., Deutsch, F., Van Looy, S.,
764 Peelaerts W., Lefebre, F., 2011. Validation of the MIMOSA-AURORA-IFDM model chan for
765 policy support: Modeling concentrations of elemental carbon in Flanders. Atmospheric
766 Environment 45, 6705-6713.
767 Lonati, G., Pirovano, G., Sghirlanzoni, G.A., Zanoni, A., Speciated fine particulate matter in
768 Northern Italy: A whole year chemical and transport modelling reconstruction, Atmospheric
769 Research, Volume 95, Issue 4, March 2010, Pages 496-514.
770 Martins, H., 2012. Urban compaction or dispersion? An air quality modelling study. Atmospheric
771 Environment 54, 60-72.
772 Monin, A. S. and Obukhov, A. M..: 1954, 'Basic Laws of Turbulent Mixing in the Ground Layer of
773 the Atmosphere', Trans. Geophys. Inst. Akad. Nauk. USSR 151, 163–187.
774 Morfeld, P., Groneberg, D.A., Spallek, M.F., 2014. Effectiveness of Low Emission Zones: large
775 scale of changes in environmental NO2, NO and NOx concentrations in 17 German cities. Plos
776 One 9,8.

Morrison, H., Thompson, G., Tatarskii, V., 2009: Impact of Cloud Microphysics on the Development of Trailing Stratiform Precipitation in a Simulated Squall Line: Comparison of One- and Two-Moment Schemes. American Meteorological Society, 137, 991- 1007.

Nenes, A, Pilinis, C., Pandis, S.N., 1998, ISORROPIA: A New Thermodynamic Model for Multiphase Multicomponent Inorganic Aerosols. Aquatic Geochemistry, 4, 123-152.

O'Brien, J.J., 1970. A note on the vertical structure of the eddy exchange coefficient in the planetary boundary layer. Journal of the atmospheric science 27, 1213-1215.

Pernigotti, D., Thunis, P., Cuvelier, C., Georgieva, E., Gsella, A., De Meij, A., Pirovano, G., Balzarini, A., Riva, G.M., Carnevale, C., Pisoni, E., Volta, M., Bessagnet, B., Kerschbaumer, A., Viaene, P., De Ridder, K., Nyiri, A., Wind, P., 2013. POMI: a model inter-comparison exercise over the Po Valley. Air Qual Atmos Health. DOI 10.1007/s11869-013-0211-1.

Skamarock, W.C., Klemp, J.B., Dudhia, J., Gill, D.O., Barker, D.M., Duda, M.G., Huang X.-Y., Wang, W., Powers, J.G., 2008. A Description of the Advanced Research WRF Version 3, NCAR Technical Note NCAR/TN-475+STR, Boulder, Colorado.

Stein, A.F., Isakov, V., Godowitch, J., Draxler, R R., 2007. A hybrid modeling approach to resolve pollutant concentrations in an urban area. Atmospheric Environment 47, 9410-9426.

Stocker J., Hood C., Carruthers D., Seaton M., Johnson K., The development and evaluation of an automated system for nesting adms-urban in regional photochemical models. 13th Annual CMAS Conference, Chapel Hill, NC, October 27-29, 2014

Torras Ortiz, S., Friedrich, R., 2013. A modelling approach for estimating background pollutant concentrations in urban areas. Atmospheric Pollution Research 4, 147-156.

UNC, 2013. SMOKE v3.5 User's manual. Available at: http://www.smoke-model.org/index.cfm.

Yarwood G., Morris, R.E., Wilson, G.M., 2004. Particulate Matter Source Apportionment Technology (PSAT) in the CAMx Photochemical Grid Model. Proceedings of the 27th NATO/ CCMS International Technical Meeting on Air Pollution Modeling and Application. Springer Verlag.

Yarwood, G., Rao, S., Yocke, M., Whitten, G., 2005. Updates to the Carbon Bond Chemical mechanism: CB05, report, Rpt. RT-0400675, US EPA, Res. Tri. Park.

7. Supplemental Material

List of statistical indices:

Mean BIAS

$$BIAS = \frac{1}{N}\sum_{t=1}^{N}\left(C_{\mathrm{mod}}(x,t) - C_{obs}(x,t)\right) = \overline{C}_{\mathrm{mod}}(x) - \overline{C}_{obs}(x)$$

Mean Absolute Error (MAE)

$$MAE = \frac{1}{N}\sum_{t=1}^{N}\left|C_{\mathrm{mod}}(x,t) - C_{obs}(x,t)\right|$$

Index of Agreement (IOA)

817
$$IA = 1 - \frac{\sum_{t=1}^{N}\left(C_{\mathrm{mod}}(x,t) - C_{obs}(x,t)\right)^2}{\sum_{t=1}^{N}\left(\left|C_{\mathrm{mod}}(x,t) - \overline{C}_{obs}(x)\right| + \left|C_{obs}(x,t) - \overline{C}_{obs}(x)\right|\right)^2}$$

818 ***Root Mean Square Error (RMSE)***

819
$$RMSE = \sqrt{\frac{1}{N}\sum_{t=1}^{N}\left(C_{\mathrm{mod}}(x,t) - C_{obs}(x,t)\right)^2}$$

820 ***Correlation (CORR)***

821
$$r = \frac{\sum_{j=1}^{N}\left(C_{\mathrm{mod}}(x,t) - \overline{C}_{\mathrm{mod}}(x)\right)\cdot\left(C_{obs}(x,t) - \overline{C}_{obs}(x)\right)}{\sqrt{\sum_{j=1}^{N}\left(C_{\mathrm{mod}}(x,t) - \overline{C}_{\mathrm{mod}}(x)\right)^2}\cdot\sqrt{\sum_{j=1}^{N}\left(C_{obs}(x,t) - \overline{C}_{obs}(x)\right)^2}}$$

822
823
824 Where:
825 $\boldsymbol{C_{mod}(x,t)}$ = modelled concentration for specific site *x* at time *t* (upper line indicates mean variable
826 for all period)
827 $\boldsymbol{C_{obs}(x,t)}$ = observed concentration for specific site *x* at time *t* (upper line indicates mean variable for
828 all period)
829 $\boldsymbol{N}$ = number of cases.
830
831 **Table S 1. Lambert Conformal coordinates for nested domains in WRF and CAMx model**

	WRF (Europe)	*WRF CAMx (Italy)*		*WRF CAMx (Po Valley)*		*WRF CAMx (Milan area)*	
SW X corner [km]	-2164.7	-634.5	-604.5	-439.5	-429.5	-249.7	-246.2
SW Y corner [km]	-2358.2	-1053.5	-1023.5	-108.5	-98.5	66.8	69.8
NE X corner [km]	1705.3	715.5	685.5	160.5	150.5	-164.7	-167.8
NE Y corner [km]	1781.8	476.5	446.5	311.5	301.5	151.8	148.2
DX-DY [km]	45	15	15	5	5	1.7	1.7
N cells X [n]	86	90	86	120	116	51	47
N cells Y [n]	92	102	98	84	80	51	47

832
833 **Table S 2. List of statistics data for Q, T and WS for WRF validation analyzing ARPA stations.**

	Mixing ratio		*Temperature*		*Wind speed*	
	Po Valley	*Milan area*	*Po Valley*	*Milan area*	*Po Valley*	*Milan area*
Num. Obs	669929	94022	1388928	97864	664066	24427
Mean OBS	7.4	7.0	285.2	285.4	1.9	1.3
Mean MODEL	7.5	7.2	284.6	286.1	2.2	1.7
CORR	0.95	0.94	0.96	0.98	0.52	0.51
Mean BIAS	0.11	0.22	-0.59	0.67	0.3	0.47
MAE	0.86	0.84	1.97	1.57	1.1	0.82
IOA	0.95	0.94	0.96	0.98	0.34	0.2
RMSE	1.2	1.23	2.68	2.01	1.48	1.1

834

Table S 3. List of statistics data for Q, T and WS for WRF validation analyzing WMO stations.

	Mixing ratio		*Temperature*		*Wind speed*	
	Po Valley	*Milan area*	*Po Valley*	*Milan area*	*Po Valley*	*Milan area*
Num. Obs	227684	24495	228958	24688	168539	12747
Mean OBS	7.6	7.3	285.2	285.7	3.1	2.8
Mean MODEL	7.6	7.5	284.7	286.5	2.6	1.6
CORR	0.94	0.97	0.95	0.98	0.53	0.5
Mean BIAS	-0.09	0.19	-0.45	0.71	-0.28	-0.9
MAE	1.02	0.71	2.12	1.41	1.47	1.19
IOA	0.94	0.96	0.95	0.98	0.45	0.28
RMSE	1.46	0.97	3.05	1.86	2	1.52

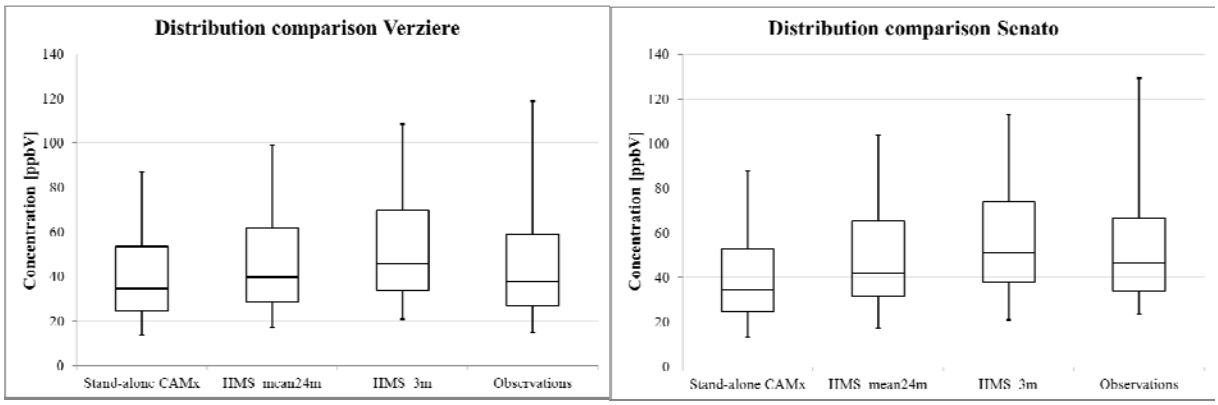

Figure S 1. Box plot comparison of measured and modeled NO_X hourly concentrations for Senato (left) and Verziere (right) site. Horizontal black line represents median value of the distributions. The box limits indicate 25th and 75th percentile. Vertical lines link 5th and 95th percentiles.

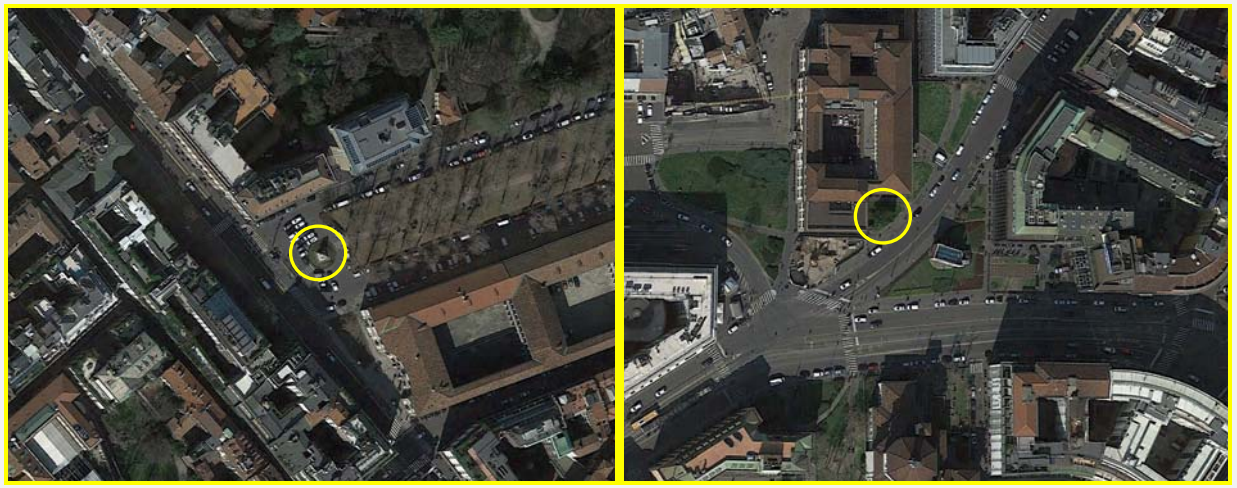

Figure S 2. Plant view of the two monitoring stations, circled in yellow. Senato site (left) and Verziere site (right).

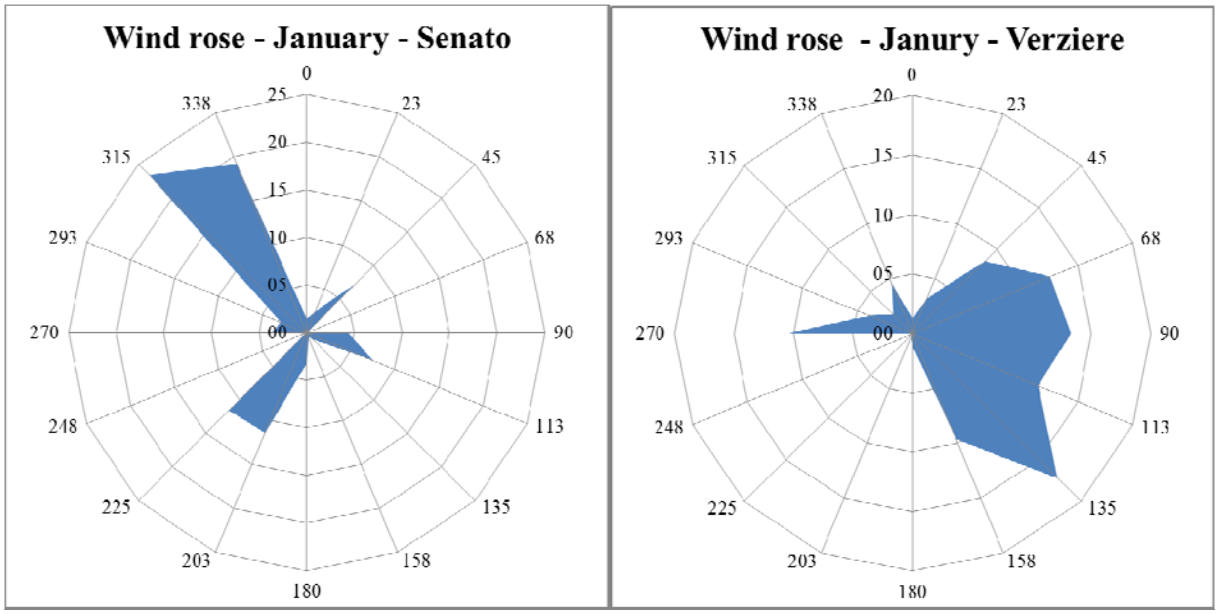

Figure S 3. Wind roses for January obtained by TALdia for two monitoring sites: Senato (left) and Verziere (right).

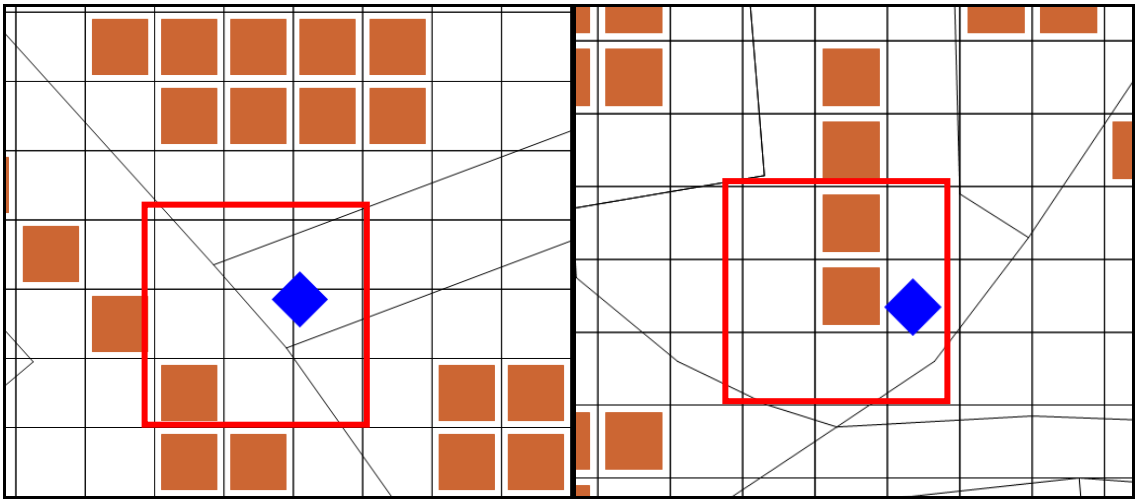

Figure S 4. Building pattern (brown box) and linear sources (black line) localization near two monitoring sites (blue square). Senato site (left) and Verziere site (right)

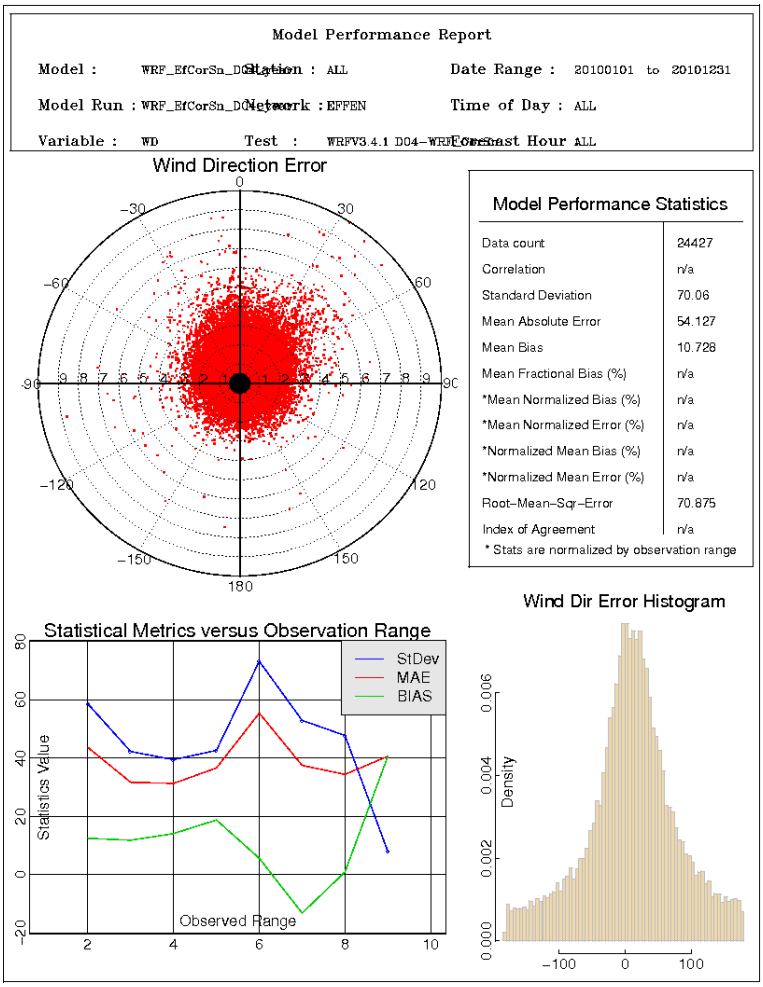

Figure S 5. Evaluation of wind direction performance over Milan area in 2010. The scatter plot (top-left) presents the distribution of the wind direction error. The x-axis represents the wind speed and on the round axis there is the wind direction error. The table (top-right) lists the principal statistical parameters. The graph "Statistical Metrics versus Observation Ranges" (bottom-left) illustrates the BIAS, MAE and StDev trend for different wind speed. The histogram (bottom-right) shows the distribution of the wind direction error probability (x-axis: positive and negative wind direction error).

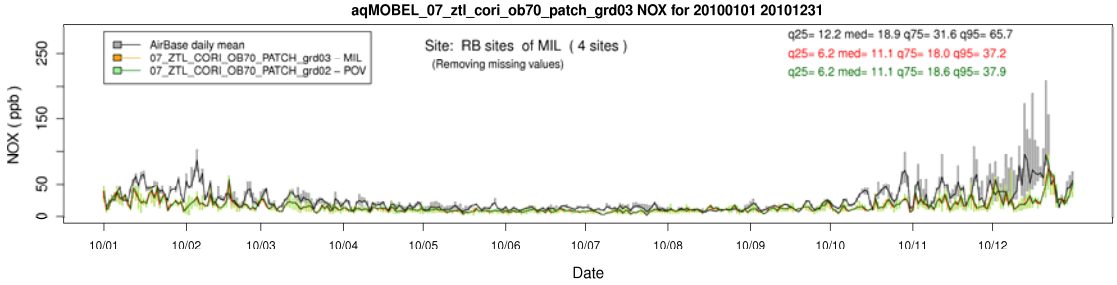

Figure S 6. Time series of the box and whisker plots for the daily distribution of the observed (black/grey) and computed values of NO_X concentration (ppb) at Rural monitoring sites of the Milan area domain for 2010. CAMx results at 5 km and 1.7 km resolution are displayed in red/orange and in green, respectively. Bars show the interquartile range, lines the median values. Values for the 25th, 50th, 75th, and 95th quantiles of the whole monthly time series are reported too.

Table S 4. Comparison of stand-alone CAMx model performance for NO_X hourly concentrations computed for 2010 at rural AQ stations of Po Valley and Milan area domain.

	Po Valley		*Milan area*	
	Observations	Model	Observations	Model
Mean [ppbV]	16.5	10.3	26.1	14.1
Standard Deviation [ppbV]	19.6	10.9	28.8	15.7
Number Observations [-]	310495		32262	
Correlation [-]	0.5		0.4	
Mean Bias [ppbV]	-6.2		-6.8	
Mean Error [ppbV]	10.2		9.2	
Index_of_Agreement [-]	0.6		0.6	
RMSE [ppbV]	18.4		29	

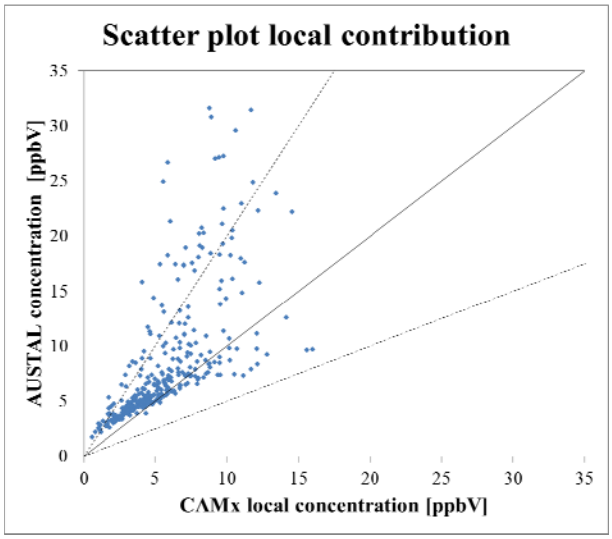

Statistical parameters	*AUSTAL2000*	*CAMx local*
Mean [ppbV]	8.55	5.61
St. Dev [ppbV]	7.55	3.03
25th percentile [ppbV]	4.54	3.40
50th percentile [ppbV]	5.96	4.87
75th percentile [ppbV]	9.27	7.21

Figure S 7. Scatter plot (left) between local daily contribution estimated by CAMx and AUSTAL outcomes for 2010. The solid black line indicates 1:1 ratio between the two models, the dashed lines represent 1:2 and 2:1 ratio. The table (right) shows the mean, the standard deviations and the 3 quartiles for the local daily contributions.

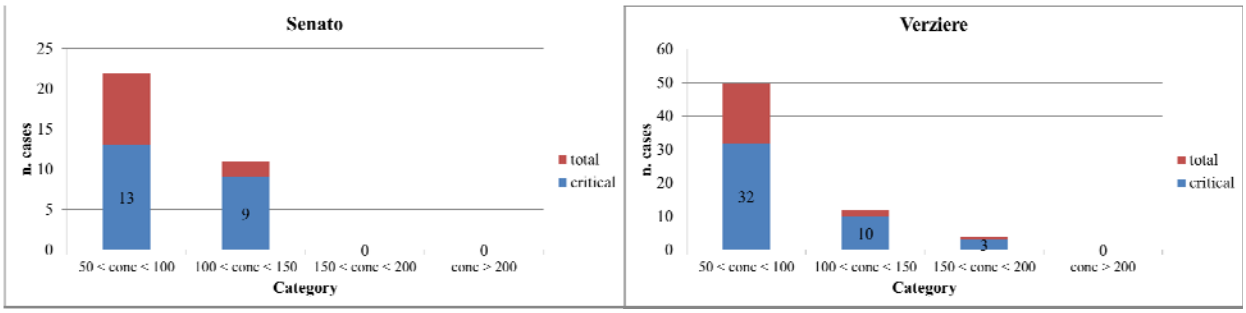

Figure S 8. Statistical distribution of the AUSTAL2000 hourly concentration, computed at two observation sites. Bars shows the number of total and critical meteorological conditions for January 2010. The "critical conditions" are defined as: wind speed < 1.5 m/s and 0.1 m < L < 50 m. The figure shows 4 categories, starting from 50 ppbV, with a 50 ppbV step size.